Understanding fragility in supercooled Lennard-Jones mixtures. II. Potential energy surface

D. Coslovich and G. Pastore
Dipartimento di Fisica Teorica, Università di Trieste – Strada Costiera 11, 34100 Triesta, Italy and CNR-INFM Democritos National Simulation Center – Via Beirut 2-4, 34014 Trieste, Italy

(Received 23 April 2007; accepted 27 July 2007; published online 26 September 2007)

The connection between isobaric fragility and the properties of high-order stationary points of the potential energy surface in different supercooled Lennard-Jones mixtures was investigated. The increase of effective activation energies upon supercooling appears to be driven by the increase of average potential energy barriers measured by the energy dependence of the fraction of unstable modes. Such an increase is sharper, the more fragile the mixture. Correlations between fragility and other properties of high-order stationary points, including the vibrational density of states and the localization features of unstable modes, are also discussed. © *2007 American Institute of Physics*. [DOI: 10.1063/1.2773720]

I. INTRODUCTION

The study of the potential energy surface (PES), or energy landscape, of supercooled liquids and glasses is of fundamental importance for understanding thermodynamical and dynamical properties in these systems.[1,2] Since the pioneering work of Stillinger and Weber,[3] a growing body of data, coming from numerical simulations, has provided a detailed description of the energy landscape explored by supercooled liquids. As the temperature is lowered toward the glass transition, progressively deeper regions of the PES are visited,[4] where the basins of attraction of groups of local minima (metabasins)[5] act as traps for the system in configuration space[6–9] and slow down the liquid dynamics. Accordingly, viscosity and structural relaxation times show a dramatic increase upon supercooling. In the so called fragile glass-formers, such an increase is faster than Arrhenius (or super-Arrhenius), as opposed to the behavior of strong glass-formers, in which the temperature dependence of transport coefficients roughly follows the Arrhenius law.

Schematic descriptions of the PES have often been invoked to explain the fragile vs. strong behavior of supercooled liquids.[10] Strong glass-formers are expected to have a rough energy landscape, with energy barriers whose amplitude is essentially independent of the energy level. On the other hand, fragile glass-formers should display a more complex organization of stationary points and a broader distribution of energy barriers. Understanding, at a quantitative level, the varying degree of fragility in different glass-formers represents a formidable task for theories. Correlations between fragility and statistical or vibrational properties of local minima of the PES (Refs. 11 and 12) have recently received a critical assessment for a wide range of models of the PES.[13] Variations in the properties of the PES explored by supercooled liquids at different densities have also been discussed,[11] but their correlation to fragility has been a matter of debate.[14] Detailed studies have focused on the role of elementary rearrangements between adjacent local minima through transition states, both at constant density[15] and constant pressure.[16] Here, we will concentrate our attention on the properties of high-order stationary points of the PES, whose relevance for supercooled liquids has been emphasized in the last years.[17–23] High-order stationary points could offer a simple explanation of the fragile behavior of glass-formers, in terms of an increase of average energy barriers.[24] This feature is encoded, in an effective way, in a number of models of energy landscapes developed in the last years,[25–28] and has sometimes been addressed in numerical simulations.[29]

Statistical properties of high-order stationary points of the PES have been investigated recently for a variety of monoatomic and binary systems, both in the liquid[30,31] and supercooled regime.[17,32] The existence of some universal features in the energy landscape of different model liquids[17,32] has been highlighted. At least in the case of the modified soft-sphere mixtures studied in Ref. 32, such a universality has been found to reflect a fragility invariance of the systems investigated.[33] In this work, we take a complementary point of view and ask: Are there *variations* in the properties of high-order stationary points which correlate to fragility? To address this point, we consider a set of Lennard-Jones mixtures cooled at constant pressure: a series of equimolar, additive mixtures with varying size ratio, together with some well-studied binary mixtures (Sec. II). By investigating the temperature dependence of effective activation energies for relaxation (Sec. III), we provide support for our previous results,[34] which indicated the existence of systematic variations of isobaric fragility in additive mixtures and a remarkable pressure invariance in the mixture of Kob and Andersen.[35,36] These trends allow us to test the connection between fragility and some statistical properties of stationary points of the PES (Sec. IV). In particular, we show how fragility can be reflected in the saddles' density of states, average energy barriers, and localization properties of unstable modes.

II. MODELS AND SIMULATION TECHNIQUES

The binary mixtures studied in this work consist of N classical particles interacting via the Lennard-Jones potential

$$u_{\alpha\beta}(r) = 4\epsilon_{\alpha\beta}\left[\left(\frac{\sigma_{\alpha\beta}}{r}\right)^{12} - \left(\frac{\sigma_{\alpha\beta}}{r}\right)^{6}\right], \quad (1)$$

where $\alpha,\beta=1,2$ are indexes of species. Each system is enclosed in a cubic box with periodic boundary conditions. In the following, reduced Lennard-Jones units will be used, i.e., σ_{11}, ϵ_{11}, and $\sqrt{m_1\sigma_{11}^2/\epsilon_{11}}$ as units of distance, energy, and time, respectively. Most simulations have been performed for samples of $N=500$ particles, employing the cutoff scheme of Stoddard and Ford[37] at a cutoff radius $r_c=2.5$. This cutoff scheme (QS) adds a shift and a quadratic term to the potential in order to ensure continuity up to the first derivative of $u_{\alpha\beta}$ at $r=r_c$. The role of the continuity of derivatives at the cutoff radius r_c has been discussed in connection with minimization procedures.[38] To further investigate this point, we have also tested cut-and-shifted (CS) and cubic-splined cutoff (CSPL) (Ref. 29) on smaller samples composed of $N=108$ particles. In this case, a slightly smaller value of the cutoff radius has been used ($r_c=2.2$).

We will focus our attention on the following binary Lennard-Jones mixtures: (i) The BMLJ mixture of Kob and Andersen,[35] probably the most widely employed model for numerical simulations of the glass-transition. (ii) The WAHN mixture of Wahnström,[39] which is another well-studied model glass-former. (iii) A set of additive, equimolar mixtures called AMLJ-λ, characterized by different values of size ratio $\lambda=\sigma_{22}/\sigma_{11}$. In this case, the size ratio is varied in the range $0.60\leq\lambda\leq0.82$. A summary of all interaction parameters, together with a more detailed description of these models, can be found in Ref. 34.

Molecular dynamics simulations were performed by cooling the liquid at constant pressure using the Berendsen thermostat and barostat during the equilibration phase. Standard velocity-Verlet algorithm was used to integrate the equations of motion. In order to achieve better control of temperature in the deeply supercooled regime, we performed a few production runs using the Nosé-Poincaré thermostat.[40,41] The time step δt was varied between 0.002 at high temperature and 0.006 at low temperature. The time constant for the Berendsen thermostat[42] was $t_T=\delta t/0.1$, while the coupling constant for the Berendsen barostat[42] was 10^3 in reduced units. The inertia parameter of the Nosé-Poincaré thermostat was set to $Q=5$. Constant pressure simulations provide a means to compare different mixtures in a way similar to the one employed in experiments. There is also interest in understanding how the sampling of the energy landscape changes when isobaric quenches are considered instead of isochoric ones.[16] The density variations along isobaric quenches at a pressure $P=10$ are shown for a selection of mixtures in Figs. 1 and 2. In order to make a comparison with standard constant density simulations, we also performed some isochoric quenches for BMLJ and WAHN by fixing the density at the value used in the original papers. A summary of our thermal histories is shown in Table I. For further details about quenching protocols see Ref. 34.

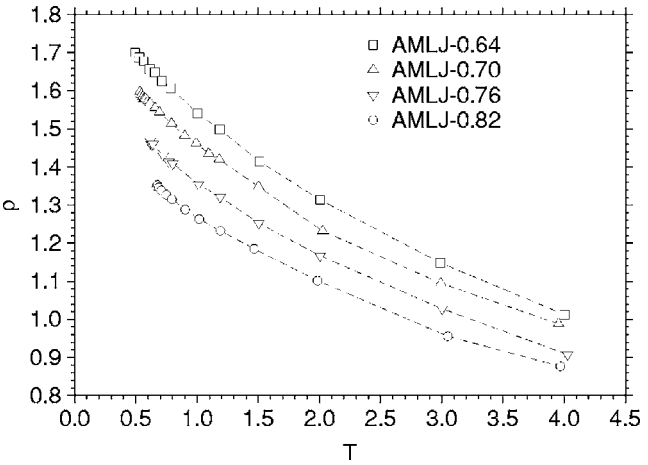

FIG. 1. Temperature dependence of density $\rho(T)$ along isobaric quenches at $P=10$ for a selection of AMLJ-λ mixtures. From bottom to top: $\lambda=0.82$, 0.76, 0.70, 0.64.

Description of the minimization technique employed for locating stationary points of the PES requires some further comments. We followed a simple and popular approach,[17] which consists of minimization of the mean square total force W of the system, using the L-BFGS algorithm.[43] For each state point, some hundreds of independent configurations (typically between 200 and 1000) from simulation runs were considered as starting points for W minimizations. Some care has to be taken, since this numerical procedure often leads to quasisaddles, i.e., points with small but nonzero W, which display an inflection mode.[17–19] As a criterion for distinguishing true saddles we use $W\lesssim W_0\equiv10^{-12}$, similarly to previous studies.[17,44] The fraction of true saddles sampled in small-sized samples ($N=108$) is rather large (from 10% to 30% for WAHN, from 5% to 20% for BMLJ, depending on temperature), so that this approach appears to be quite feasible for similar system sizes. For larger samples, the fraction of true saddles decreases. However, from an overall point of view, our findings indicate that saddles and quasisaddles share similar average properties, in agreement with several previous observations.[17,20,38] We also found that ensuring continuity of the interaction potential up to the first

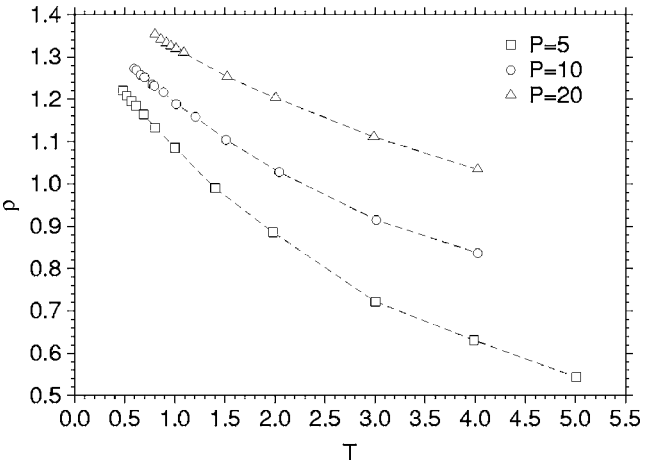

FIG. 2. Temperature dependence of density $\rho(T)$ along isobaric quenches at for BMLJ at $P=5$, $P=10$, and $P=20$.

TABLE I. Summary of thermal histories and simulation details. Also shown are the number concentration of large particles x_1, the cutoff scheme used (see the text for definitions), and the value of the cutoff radius r_c. In the case of AMLJ-λ mixtures, the following values of λ have been considered: λ=0.60, 0.64, 0.70, 0.73, 0.76, 0.82.

	N	x_1	P	Cutoff	r_c
			Isobaric quenches		
BMLJ	108	0.8	10	QS	2.2
	108	0.8	10	CS	2.2
	108	0.8	10	CSPL	2.2
	500	0.8	5	QS	2.5
	500	0.8	10	QS	2.5
	500	0.8	20	QS	2.5
	500	0.8	50	QS	2.5
WAHN	108	0.5	10	QS	2.2
	500	0.5	10	QS	2.5
	500	0.5	20	QS	2.5
AMLJ-λ	500	0.5	10	QS	2.5
			Isochoric quenches		
BMLJ	500	0.8	1.2	QS	2.5
WAHN	500	0.5	1.3	QS	2.5

derivative at $r=r_c$, i.e., employing the QS cutoff, is enough to avoid major round-off errors in W minimizations. Moreover, the fraction of true saddles sampled for $N=108$ does not increase appreciably when using the smoother CSPL cutoff.

III. EFFECTIVE ACTIVATION ENERGIES

A common way to display the temperature dependence of structural relaxation times $\tau(T)$ in supercooled liquids is by construction of the so-called Angell plot, in which log τ is shown against T_g/T. In a previous work,[34] we used a similar approach to analyze the variations of fragility in Lennard-Jones mixtures. Here, we take a different view of the same problem and analyze the effective activation (free) energy $E(T)$ defined by inversion of

$$\tau(T) = \tau_\infty \exp\left[\frac{E(T)}{T}\right], \tag{2}$$

where τ_∞ is the high-temperature limit of relaxation times. Analysis of the temperature dependence of $E(T)$ will allow us to make contact with previous work based on effective activation energies,[45] and to discuss the variation of fragility in a way more convenient for highlighting the role of the PES (Sec. IV).

Experimental and numerical analysis of effective activation energies $E(T)$ in supercooled liquids clearly signals a crossover between two distinct dynamical regimes. At high temperature, relaxation times follow a mild, Arrhenius-type temperature dependence, $\tau_\infty \exp[E_\infty/T]$. Hence, in the normal liquid regime, we have $E(T)\approx E_\infty$. Below some crossover temperature T^*, effective activation energies of fragile glass-formers increase markedly, indicating super-Arrhenius behavior. The more fragile the glass-former, the shaper the increase of effective activation energies below T^*. The features of $E(T)$ just discussed are incorporated in the so-called frustration-limited domains theory of the glass-transition,[14] which predicts $E(T)$ to be of the form

$$E(T) = \begin{cases} E_\infty & T > T^* \\ E_\infty + BT^*\left(1 - \frac{T}{T^*}\right)^{8/3} & T < T^* \end{cases} . \tag{3}$$

It has been shown[45] that the functional form in Eq. (3) provides a fair account of a wide spectrum of experimental data. Fragility is measured by B, which is the parameter quantifying the departure from the high-temperature Arrhenius regime. Further discussions on the role of the other parameters in Eq. (3) and on the exponent 8/3 can be found in Refs. 46 and 47.

The dynamical quantity on which we focus in this section is the relaxation time for the decay of density fluctuations, as identified by the self-part of the intermediate scattering function $F_s^\alpha(k,t)$, where $\alpha=1,2$ is an index of species. We define relaxation times τ_α by requiring that $F_s^\alpha(k^*,t)$ has decayed to $1/e$, where $k^*\approx 8$ is the position of the first maximum in the number-number static structure factor of the mixtures in consideration.[34] A first guess of the crossover temperature T^* is provided by the temperature T_{onset} at which two-step, nonexponential relaxation of $F_s^\alpha(k,t)$ is first observed upon cooling the liquid from high temperature.[36] For fitting our data to Eq. (3), we proceed as suggested by Kivelson *et al.*[45] First we fit the high-temperature portion of our data ($T>T_{\text{onset}}$) to an Arrhenius law $\tau_\infty \exp[E_\infty/T]$, and then we use τ_∞ and E_∞ as fixed parameters in global a fit of our simulation data to Eq. (3). Note that, although T^* is considered as a fitting parameter, its final value is never too far from the initial guess T_{onset}.

In Table II, we summarize the results of our fitting procedure for Eq. (3). Considering separately the cases of effective activation energies for large and small particles, we find that the fitted parameters for the two species show similar trends of variation in different systems and for different pres-

TABLE II. Parameters of fits to Eq. (3) for effective activation energies $E(T)$ of large and small species. The reference temperature T_r and the onset temperature T_{onset} are described in the text.

			Large particles				Small particles			
	P	T_r	T^*	B	τ_∞	E_∞	T^*	B	τ_∞	E_∞
BMLJ	5	0.464	0.83(2)	33±5	0.0931(3)	1.99(1)	0.81(1)	40±5	0.097(1)	1.62(3)
BMLJ	10	0.574	1.05(1)	29±3	0.0815(5)	2.61(1)	1.06(1)	30±2	0.0889(9)	1.93(2)
BMLJ	20	0.765	1.41(4)	26±4	0.067(1)	3.71(9)	1.44(4)	26±4	0.0733(8)	2.69(3)
BMLJ	50	1.248	2.27(5)	28±4	0.0481(9)	6.60(7)	2.35(5)	27±3	0.052(1)	4.7(1)
WAHN	10	0.623	0.94(1)	77±11	0.0825(4)	2.33(1)	0.91(1)	91±12	0.0567(3)	2.44(1)
WAHN	20	0.825	1.23(2)	82±15	0.0670(6)	3.38(3)	1.20(2)	96±15	0.0455(3)	3.57(3)
AMLJ-0.60	10	0.451	0.92(2)	20±2	0.076(1)	2.43(3)	0.91(1)	18±1	0.0828(7)	1.69(2)
AMLJ-0.64	10	0.474	0.88(1)	27±3	0.076 91(3)	2.444(1)	0.88(1)	25±2	0.0834(4)	1.76(1)
AMLJ-0.70	10	0.514	0.86(2)	46±9	0.0811(1)	2.359(4)	0.84(2)	49±9	0.084(1)	1.84(5)
AMLJ-0.73	10	0.560	0.82(1)	94±16	0.0785(7)	2.48(2)	0.84(1)	86±14	0.0839(7)	1.93(2)
AMLJ-0.76	10	0.601	0.84(1)	128±22	0.0790(9)	2.49(3)	0.85(1)	120±20	0.083(1)	2.00(5)
AMLJ-0.82	10	0.636	0.90(1)	100±18	0.0803(5)	2.53(1)	0.92(1)	92±16	0.0829(8)	2.17(2)
BMLJ	1.2	0.422	0.77(1)	22±3	0.110(2)	2.69(2)	0.85(1)	17±2	0.0909(7)	2.25(1)
WAHN	1.3	0.522	0.81(1)	65±6	0.097(1)	2.73(2)	0.81(1)	61±6	0.071(1)	2.70(3)

sure and density conditions. In the following, we will thus simply focus on the effective activation energies $E(T)$ obtained from the relaxation times $\tau \equiv \tau_1$ of large particles. In order to put into evidence the variation of fragility index B for different mixtures we plot, as in Ref. 14, the difference $(E(T)-E_\infty)/T^*$ against the reduced temperature T/T^*. In Fig. 3, we show results obtained along isobaric quenches at $P=10$ for a selection of AMLJ-λ mixtures (upper plot), and for BMLJ and WAHN mixtures (lower plot). The first important point is that there is a systematic variation of fragility with size ratio. Below the crossover temperature T^* effective activation energies increase faster as the size ratio λ increases, i.e., AMLJ-λ mixtures become more fragile as λ increases. The second point is that BMLJ mixture is less fragile than WAHN mixture. These observations are substantiated by the outcome of our fitting procedure. From an overall point of view, we find that Eq. (3) provides a good fitting function for our simulation data. Actually, the crossover around T^* in our simulation data is smoother than predicted by Eq. (3), but it should also be remarked that Eq. (3) is not expected to hold exactly around T^*.[45] In the inset of the upper plot of Fig. 3, the fragility parameter B is shown as a function of size ratio for AMLJ-λ mixtures. Despite the somewhat large uncertainty of our estimate of B, there is a clear trend of increase of B as λ increases and a tendency to saturate around $\lambda \approx 0.80$. Results obtained along different isobars for BMLJ show that the isobaric fragility index B for this system is essentially pressure invariant in the range $5 \leq P \leq 50$, as can be seen from the inset of the lower plot in Fig. 3.

Within the frustration-limited domains theory,[14] the crossover temperature T^* is interpreted as an intrinsic ridge between two distinct dynamical regimes, and should thus provide a means to scale and compare properties of different glass-formers. Nonetheless, the use of isochronic, conventional reference temperatures, such as the glass-transition temperature T_g, is often useful and effective.[46] We thus introduce a reference temperature T_r such that the relaxation time for large particles reaches $\tau(T_r)=4\times10^4$. Since the value τ_∞ obtained from the high-temperature behavior is roughly system independent at a given pressure, the activation energies for different systems converge to a common value $E(T_r)/T_r \approx \log(\tau(T_r)/\tau_\infty) \approx 12$ as $T \to T_r$. Thus, a plot in which both $E(T)$ and T are scaled by T_r can be regarded as a generalized Angell plot, in which activation energies for different systems, when considered along the same isobar, converge around T_r to a common value. This kind of plot is shown in Fig. 4, where we compare AMLJ-λ mixtures for different values of λ (upper plot) and the two prototypical mixtures BMLJ and WAHN (lower plot). In this representation, fragility can be seen from a more pronounced increase of effective activation energies, relative to the high-temperature limit. A rough estimate of fragility can be thus obtained from the value of E_∞/T_r, a fact which resembles the experimental correlation between E_∞/T_g and fragility.[48]

A comparative analysis, based on Eq. (3), of experimental and numerical data was attempted some years ago by Ferrer *et al.*,[46] and further discussed by Tarjus *et al.*[47] The outcome of the fitting procedure led these authors to raise some doubts about the fragile nature of some simulated models of supercooled liquids, including the BMLJ mixture. This was contrary to the expectation, based on qualitative grounds,[49] that Lennard-Jones mixtures should be fragile glass-formers. Given the variety of Lennard-Jones models and external conditions analyzed in this work, we are probably in the position to shed some light on this point. First, we note that, for *all* mixtures considered, the ratio $E(T)/E_\infty$ is already larger than 2 around T_r. We remark that this is a typical fragile behavior, even when compared to experimental data for fragile glass-formers such as *ortho*-terphenyl.[47] Note that, apart from the trivial determination of E_∞, this result is independent of the fitting procedure. Second, comparisons between experiments and numerical simulations of supercooled liquids should always be made with care. A much more limited temperature range is available in numerical simulations, and this can bias the results of fits to Eq. (3). For instance, by restricting the temperature range for fitting so that $\tau \lesssim 10^2$, we obtained for BMLJ values of fragility index as low as $B \approx 12$ at constant pressure, and $B \approx 4$ at

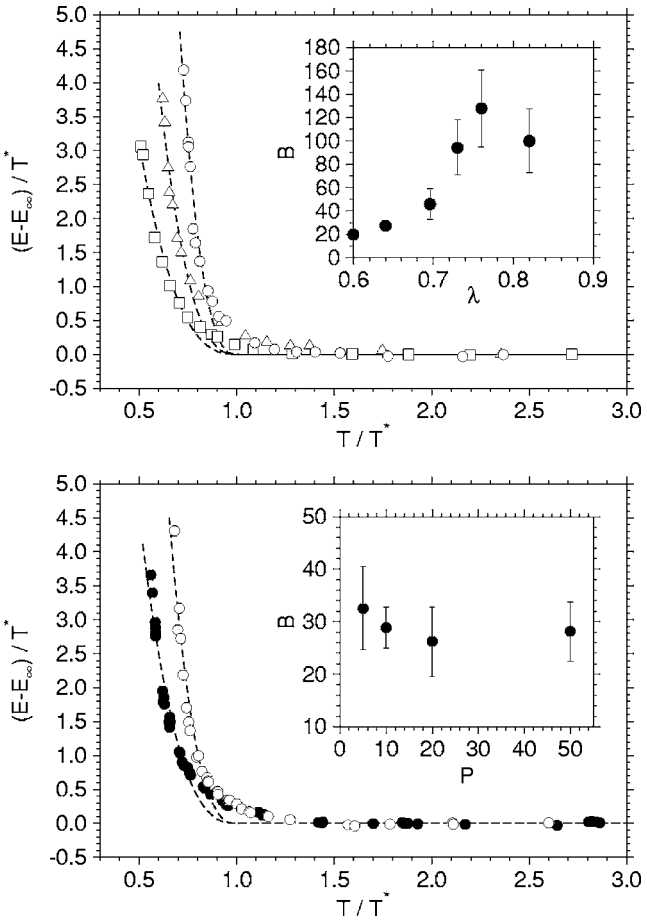

FIG. 3. Effective activation energies for relaxation of large particles, after removal of the high-temperature limit E_∞. The dependence of $(E(T)-E_\infty)/T^*$ on reduced temperature T/T^* is shown along isobaric quenches at $P=10$. Dashed lines are fits to Eq. (3). Upper plot: AMLJ-λ mixtures for values of size ratio λ=0.60 (squares), 0.70 (triangles), and 0.76 (circles). Lower plot: BMLJ (filled circles) and WAHN (open symbols). Inset of upper plot: fragility index B of AMLJ-λ vs λ. Inset of lower plot: fragility index B vs P obtained for different isobars in BMLJ.

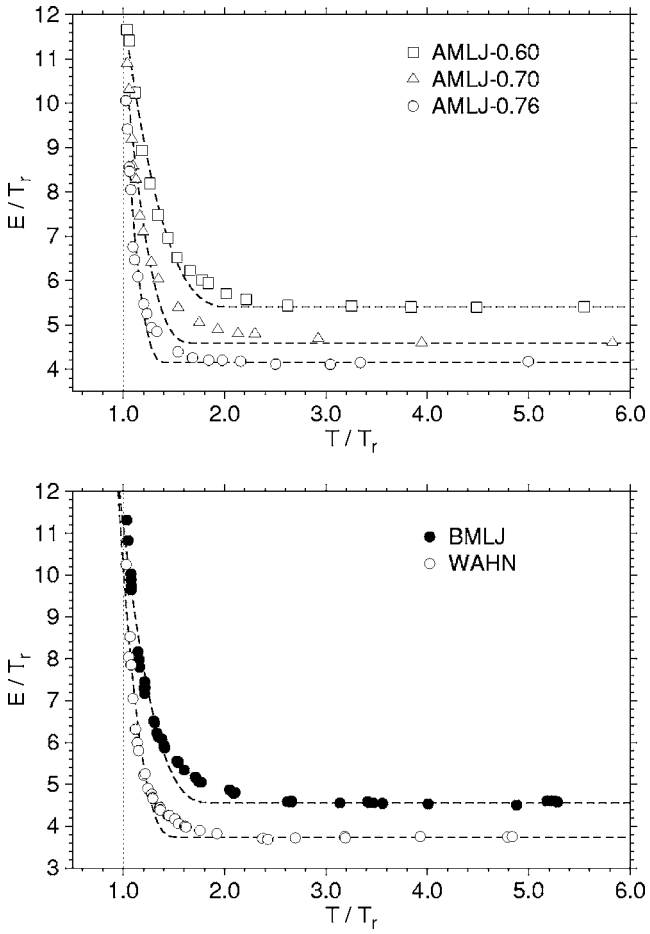

FIG. 4. Scaled effective activation energies E/T_r as a function of T/T_r, along the isobar $P=10$. Dashed lines are fits to Eq. (3). Upper plot: AMLJ-λ mixtures, for λ=0.60 (squares), λ=0.70 (triangles), and λ=0.76 (circles). Lower plot: BMLJ (filled circles) and WAHN (open circles).

constant density, in line with the results obtained in Ref. 47 by considering a similar range of τ. Fitting our data down to T_r, we obtain $B\approx 30$ for BMLJ at constant pressure, and we expect that equilibrating the system at even lower temperatures would yield slightly larger values of B. Also note that for additive Lennard-Jones mixtures with moderate size asymmetry we find $B\approx 100$, which is already typical of intermediately fragile liquids ($B\approx 90$ for glycerol).[47] Thus, from an overall point of view, Lennard-Jones mixtures appear to be fragile glass-formers, as may be expected for simple systems with nondirectional interactions. On the other hand, it is true that some Lennard-Jones mixtures are less fragile than others. In particular, the well-studied BMLJ mixture is not among the most fragile Lennard-Jones mixtures.

IV. POTENTIAL ENERGY SURFACE

An important role for understanding the dynamical features of supercooled liquids is played by stationary points of the PES and, more generally, by the negatively curved regions of the PES.[17,20–22] In this section, we will adopt a simple, nontopographic point of view, ignoring the connectivity of stationary points. Approaches based on pathways connecting adjacent minima through transition states[15,16] or transitions between metabasins[6–8] have been recently developed and applied to some model supercooled liquids, but they require expensive and complex numerical procedures. We will thus focus on some simple statistical features of the PES, and discuss their correlations to fragility in Lennard-Jones mixtures.

In the following, we will investigate the local curvature of the PES by looking at the Hessian matrix $\mathcal{H}$ of the potential energy. Standard diagonalization of $\mathcal{H}$ yields a set of $3N$ modes with eigenvalues ω_α^2 and eigenvectors $\boldsymbol{e}_j^\alpha$, where $\alpha=1,\ldots,3N$ is an index of mode and $j=1,\ldots,N$ is an index of particle. Modes are then classified as stable if ω_α^2 is positive (real frequency), or unstable if ω_α^2 is negative (imaginary frequency). For liquids, most of the relevant information is encoded in the unstable modes of the PES, whose analysis usually comes in two varieties.[66] The first approach is referred to as instantaneous normal modes (INM) analysis, and focuses on instantaneous configurations sampled along the MD trajectory.[50–52] The second approach considers high-order stationary points of the PES, obtained using minimization procedures.[17–19,21,53] According to the number of unstable modes n_u in the Hessian matrix, stationary points are classified as local minima ($n_u=0$) or saddles ($n_u\neq 0$). As

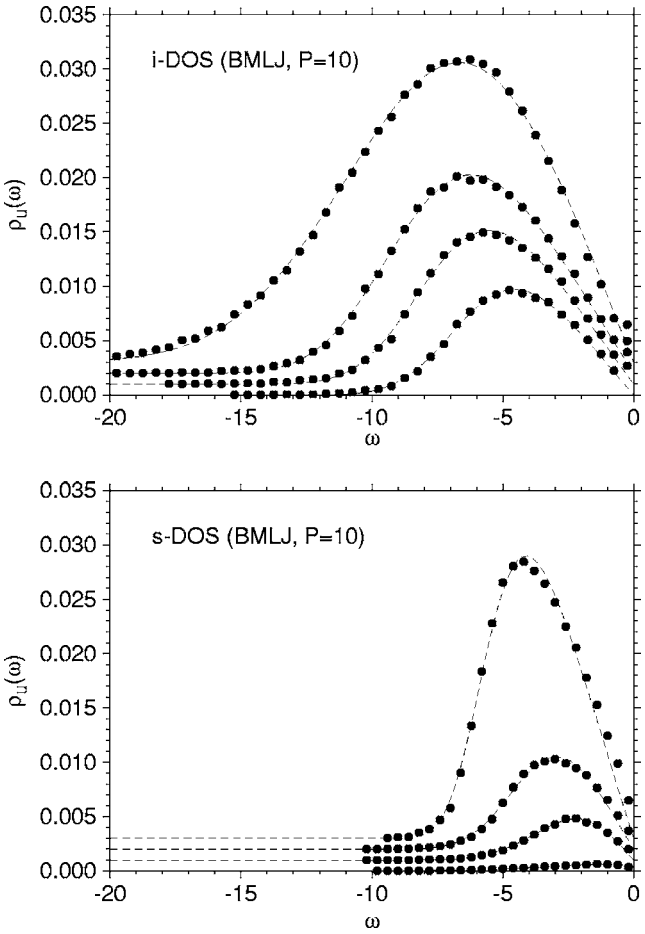

FIG. 5. Unstable branch of density of states $\rho_u(\omega)$ for instantaneous configurations (i-DOS, upper plot) and saddles (s-DOS, lower plot) in BMLJ. Results are shown at four different state points at $P=10$ (from top to bottom, $T=2.0$, 1.0, 0.7, 0.6). Dashed lines are fits to Eq. (5).

mentioned in Sec. II, quasisaddles are other points of the PES often reached by the minimization algorithm employed in this work. The exclusion of quasisaddles from statistical averages will not affect the main conclusions of this section. We checked the reliability of our results on some smaller samples of $N=108$ particles, in which a larger fraction of saddles could be found (Sec. II). In the following, we will focus on the larger sample ($N=500$) and we will mostly use the term "saddles" in a broad sense, without distinction between saddles and quasisaddles.

As a starting point, we consider the ensemble-averaged density of states (DOS),

$$\rho(\omega;T)=\left\langle \sum_{\alpha=1}^{3N}\delta(\omega_\alpha-\omega)\right\rangle_T, \tag{4}$$

at temperature T. The thermal average in Eq. (4) can be performed using either instantaneous configurations (i-DOS) or saddles (s-DOS). The unstable branch of $\rho(\omega;T)$ will be denoted by $\rho_u(\omega;T)$, and imaginary frequencies will be shown, as usual, along the real negative axis. To provide a quantitative account of the features of $\rho_u(\omega;T)$, we consider the following functional form:

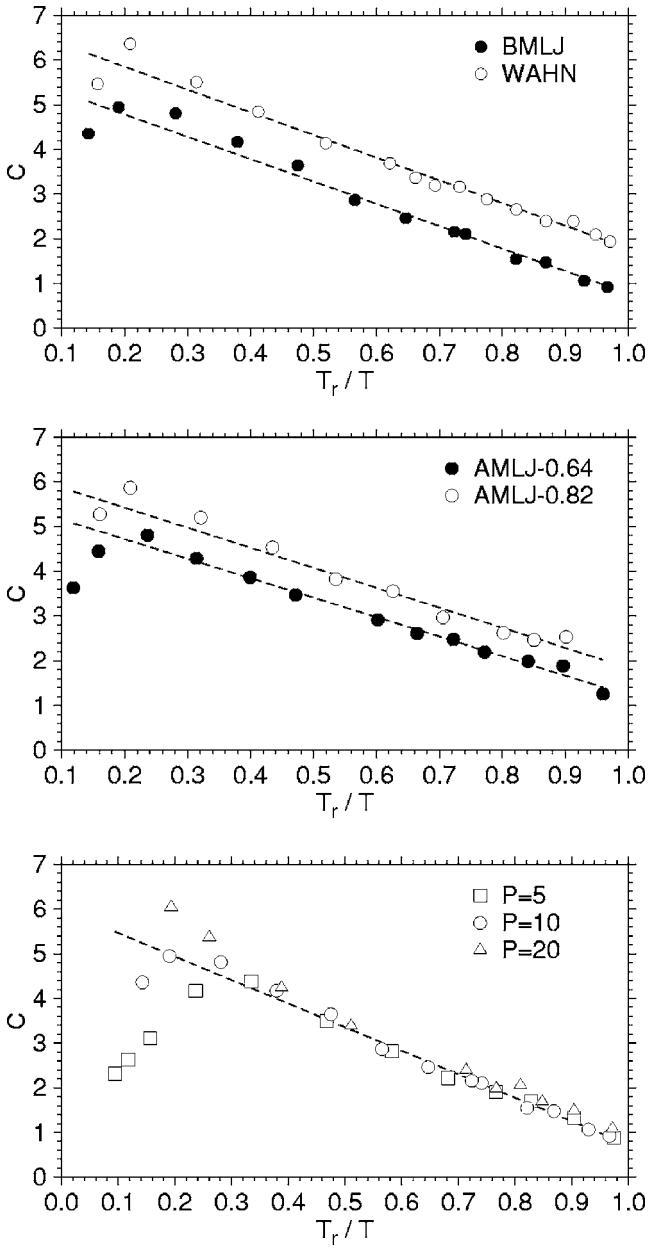

FIG. 6. Parameter C for s-DOS obtained from fits to Eq. (5) as a function of T_r/T. Upper plot: BMLJ (filled circles) and WAHN (open circles) at $P=10$. Middle plot: AMLJ-0.64 (filled circles) and AMLJ-0.82 (open circles) at $P=10$. Lower plot: BMLJ at different pressures, $P=5$ (squares), $P=10$ (circles), and $P=20$ (triangles). Dashed lines are fits of the type $a+b(T_r/T)$, with $b\approx 5$ being roughly system independent.

$$\rho_u(\omega;T)=A\omega\exp\left[\left(\frac{B\omega}{\sqrt{T}}\right)^C\right], \tag{5}$$

which has been shown to describe well the unstable i-DOS.[52] Specific functional forms for the s-DOS have been discussed, for instance, in the context of p-spin models,[28,54] but they fail to meet some basic requirements for realistic systems, such as the behavior $\rho(\omega)\to 0$ for $\omega\to 0$. We have thus attempted to apply Eq. (5) also to s-DOS and found that Eq. (5) provides an excellent fit for both i-DOS and s-DOS, becoming inadequate only at very high temperature or in the limit of vanishing interval of imaginary frequencies. The quality of the fits obtained using Eq. (5) is exemplified in Fig. 5 for

different state points of BMLJ.

In the context of the INM theory of diffusion,[55] super-Arrhenius behavior is explained in terms of the temperature dependence of the parameters in Eq. (5) for the i-DOS, and should be primarily signaled by an increase of C by decreasing temperature.[50,52,56,57] Unfortunately, we found that INM theory is not able to put into evidence the different fragility of the Lennard-Jones mixtures considered in this work.[67] For instance, we found that C, as a function of T/T_r, has similar values in all systems, whereas we would have expected a sharper increase in the case of more fragile mixtures. Analysis of the s-DOS in terms of Eq. (5) provides a different, sharper picture. Without attempting a detailed analysis of the temperature dependence of all parameters in Eq. (5), we will focus on the behavior of parameter C. In Fig. 6, we show the dependence of C on T/T_r for the s-DOS of different mixtures at constant pressure. Apart from some deviations at very high temperature, C decreases by decreasing temperature, differently from the case of the i-DOS. In all systems, we observe a temperature dependence of the type $C \sim b(T_r/T)$. Interestingly, all mixtures seem to share a common value of the slope $b \approx 5$ in a plot of C versus T/T_r, and we find a shift toward larger values of C as fragility increases. As a check of the relation between C and fragility, the values of C along different isobars for BMLJ collapse on a master curve when plotted against T/T_r, consistent with the pressure invariance of fragility reported in Sec. III. Our results thus indicate that Eq. (5) could provide a good starting point for modeling the s-DOS in realistic systems, and that a saddle-based approach is more sensitive to the dynamical behavior of supercooled Lennard-Jones mixtures than INM.

In the light of previous studies of vibrational properties of local minima,[11,15] it might be asked whether coarse-grained quantities obtained from the s-DOS, such as the average frequency of stable modes

$$\omega_s(T) = \int_{-\infty}^{0} d\omega\, \omega\rho(\omega;T), \tag{6}$$

and unstable modes

$$\omega_u(T) = \int_{0}^{\infty} d\omega\, \omega\rho(\omega;T), \tag{7}$$

already convey information about fragility. In Fig. 7, we show the dependence of ω_u and ω_s on T/T_r for different mixtures at constant pressure. We found analogous thermal behaviors by considering geometric mean frequencies of stable and unstable modes. Similar to what happens in the case of local minima,[16] constant-pressure data show an increase of ω_s by decreasing temperature, i.e., by decreasing energy of saddles. This behavior is opposite the one observed in constant-density simulations. The average frequency of unstable modes ω_u always shows a nonmonotonic temperature dependence, characterized by a maximum at intermediate temperatures, which is peculiar to isobaric quenches. Comparing mixtures along isobaric quenches at $P=10$, we find a slight shift to larger absolute vibrational frequencies as fragility decreases. However, the robustness of this correlation is weakened when it is tested using the pressure invariance of isobaric fragility in BMLJ. In the bottom plot of Fig. 7, we look at the behavior of ω_s and ω_u along different isobars in BMLJ. As the pressure P of the isobar increases, vibrational frequencies are shifted markedly to larger absolute values, most probably by the increasing density.[68] This behavior led us to reconsider the case of local minima along different isobars in BMLJ, and we found a similar trend in vibrational properties. Thus, although some correlation might

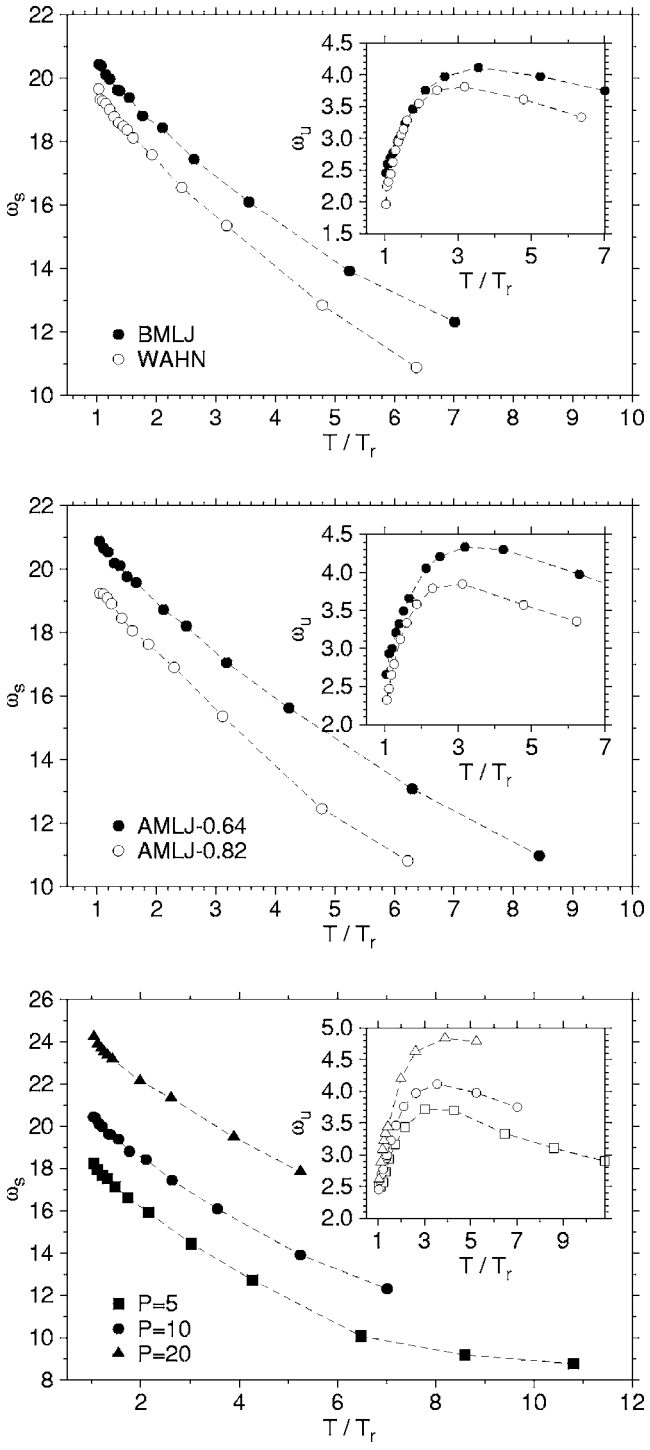

FIG. 7. Average frequency of stable modes ω_s (main plots) $\omega_u$and unstable modes (insets) of saddles as a function of T/T_r. Upper plot: BMLJ (filled circles) and WAHN (open circles) at $P=10$. Middle plot: AMLJ-0.64 (filled circles) and AMLJ-0.82 (open circles) at $P=10$. Lower plot: BMLJ at $P=5$ (squares), $P=10$ (circles), and $P=20$ (triangles).

be observed at a given pressure, there seems to be no direct connection between average vibrational frequencies of stationary points and fragility.

The variation of fragility in Lennard-Jones mixtures, as discussed in terms of effective activation energies for relaxation $E(T)$, calls for an explanation based on energy barriers. Whereas it is clear that $E(T)$ in Eq. (2) is rather an activation *free* energy, the leading contribution to it might already come from potential energy barriers between single saddles. To address this point, we follow the simple proposal of Cavagna.[24] The starting point is the relation

$$f_u = f_u(e_s), \tag{8}$$

between the fraction of unstable modes and the energy of saddles. Equation (8) will be treated as parametric in T, i.e., we consider the average fraction of unstable modes

$$f_u = f_u(T) = \langle n_u/3N \rangle_T = \int_{-\infty}^{0} d\omega\, \rho_u(\omega;T), \tag{9}$$

and the average energy of saddles

$$e_s = e_s(T), \tag{10}$$

at temperature T. It has been shown that Eq. (8), as obtained from numerical simulations, is insensitive to the actual minimization algorithm employed,[44] and to the inclusion of quasisaddles.[20] According to Cavagna,[24] the average energy difference

$$E_s(e_s) = \frac{1}{3}\frac{de_s}{df_u}, \tag{11}$$

between saddles of order n and $n+1$ provides an estimate of potential energy barriers in the PES. More refined treatments would take into account the connectivity of saddles and existence of a distribution of energy barriers.[18] In order to find $E_s(T)$, we compute the derivative in Eq. (11) by linear regression of e_s versus f_u scatter data of saddles sampled at temperature T, as illustrated in Fig. 8.

The temperature dependence of the effective energy barriers $E_s(T)$ is shown in the left plots of Fig. 9 for different mixtures at constant pressure. Below T^*, i.e., in the range of temperature where activated dynamics is expected to become important,[7,58] the behavior of $E_s(T)$ correlates with the fragility of the mixture. In fact, the increase of effective energy barriers upon supercooling is sharper and more pronounced, the more fragile the mixture. In the case of the more fragile mixtures, we find a striking similarity between the increase of $E_s(T)$ below T^* and that of the effective activation energies $E(T)$ defined by Eq. (2). In WAHN, for instance, we find $E(T_r) \approx E_s(T_r) \approx 12T_r$. The trends just discussed are in line with the results obtained by direct calculations of energy barriers between adjacent minima in the soft-sphere version of WAHN[29] and BMLJ.[7] Some concerns might regard the fact that $e_s(T)$, i.e., the energies of saddles sampled at a given T, can depend on the minimization algorithm.[44] On the other hand, the results obtained in Ref. 44 indicate that the *energy* dependence of the properties of saddles is much less sensitive to the details of the minimization procedure employed. We have thus analyzed our data for E_s as a function of e_s,

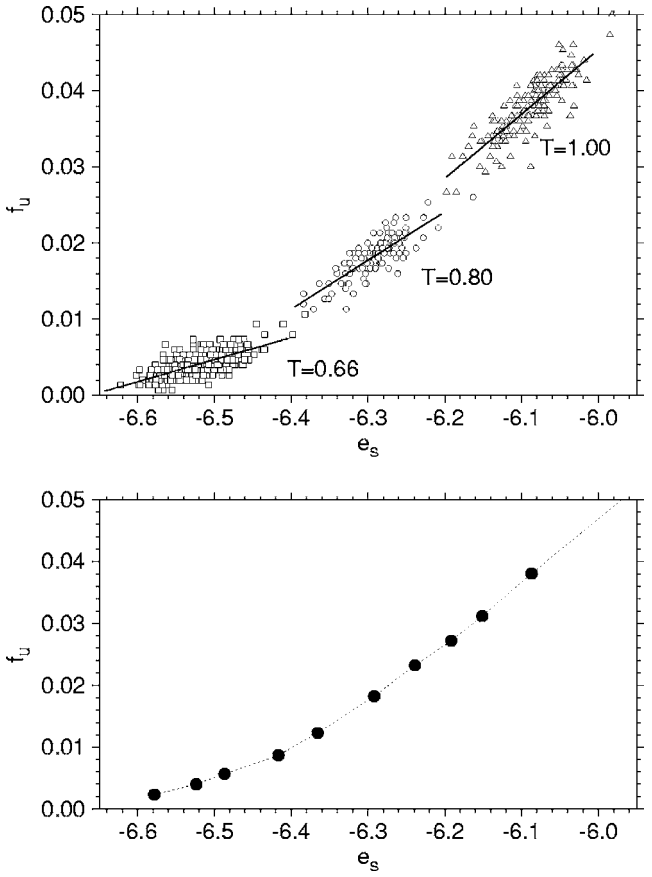

FIG. 8. Upper plot: scatter plot of the fraction of unstable modes against energy of single saddles. Results are shown for WAHN at $P=10$ for three different state points: $T=0.66$ (squares), $T=0.80$ (circles), and $T=1.00$ (triangles). Linear fits of the type $f_u=a+be_s$ (solid lines) are used to estimate the derivative in Eq. (11), i.e., $E_s=1/3b$. Lower plot: parametric plot of average unstable modes of saddles $f_u(T)$ against energy of saddles $e_s(T)$, for WAHN at $P=10$.

where e_s is given by the thermal average in Eq. (10), focusing on the energy range below $e_s(T^*)$. For convenience, we have shifted the energies e_s by $e_s(T^*)$. Such a representation of our data is shown in the right plots of Fig. 9 and confirms the trends discussed above on the basis of the temperature dependence of E_s. Thus, independent of the representation used, the average energy barriers show a strong connection to the variations of fragility in our models. This also provides evidence of the relevance, for the supercooled dynamics, of the $e_s(T)$ mapping obtained through W minimizations.

What is the effect of pressure on energy barriers? From the plot in Fig. 10, we see that increasing pressure in BMLJ leads to larger potential energy barriers. This behavior is consistent with the results obtained by Middleton and Wales,[16] who calculated the distribution of potential energy barriers for diffusive rearrangements at different pressures for BMLJ. What is made clear by our results is that, at least in the case of BMLJ, the increase of potential energy barriers with pressure has little dynamical impact, because it is compensated by the increase of the reference temperature T_r. That is, larger energy barriers will be sampled at higher temperatures. Starting from data along different isobars in BMLJ, in fact, we could obtain a rough master curve by scaling both E_s and T by T_r.

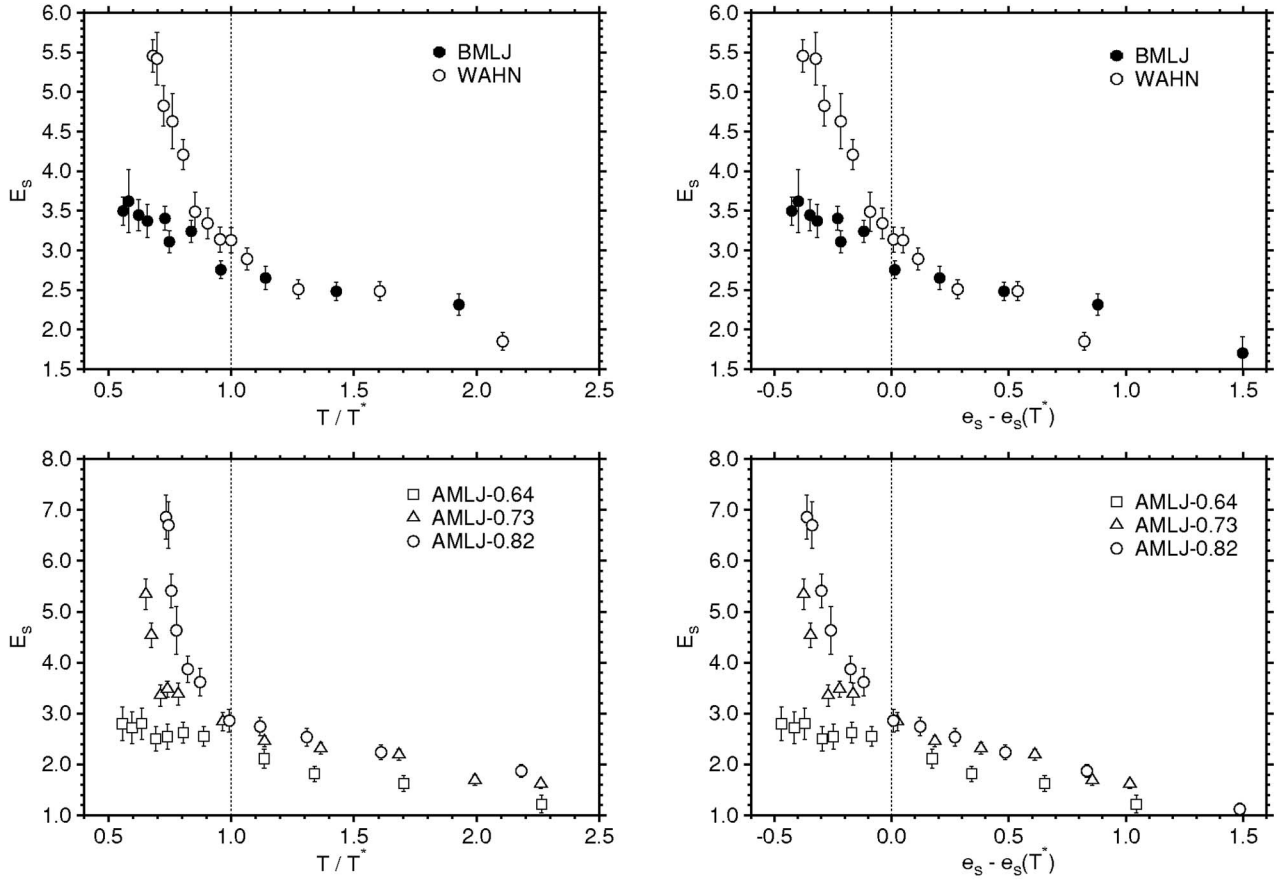

FIG. 9. Effective energy barriers E_s as a function of reduced temperature T/T^* (left column) and as a function of $e_s-e_s(T^*)$ (right column). Upper plots: WAHN (open circles) and BMLJ (filled circles) at $P=10$. Lower plots: AMLJ-0.82 (open circles) and AMLJ-0.64 (filled circles) at $P=10$.

The unstable modes of saddles sampled in the supercooled regime may provide information about the elementary dynamical processes in the system.[23] It is thus of interest to analyze the spatial localization features of unstable modes in different Lennard-Jones mixtures, and see how they relate to fragility. To address this point, we first average the squared displacements for each particle over all the unstable modes,[23]

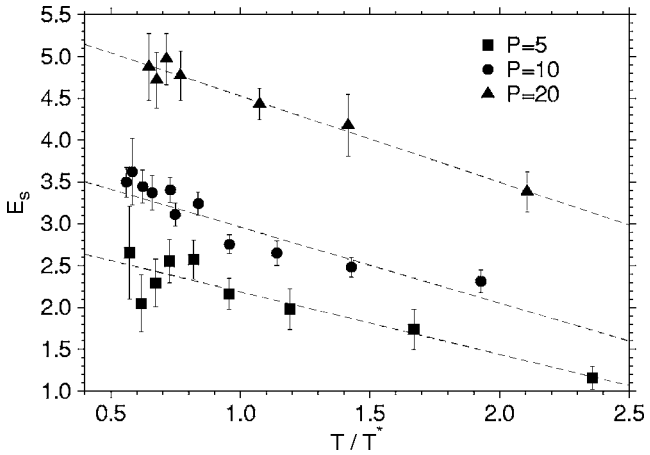

FIG. 10. Effective energy barriers E_s as a function of reduced temperature T/T^* for BMLJ at $P=5$ (squares), $P=10$ (circles), and $P=20$ (triangles). Dashed lines represent linear fits.

$$E_i^{u2} = \frac{1}{n_u} \sum_{\alpha=1}^{n_u} \boldsymbol{e}_i^{\alpha 2}. \tag{12}$$

Two different measures of localization for the vector of average squared displacements E_i^{u2} are then considered. The reduced gyration radius is defined as

$$L^u = \frac{1}{L/2} \left[\sum_{i=1}^{N} |\boldsymbol{r}_i - \boldsymbol{r}_g|^2 E_i^{u2} \right]^{1/2}, \tag{13}$$

where L is the side of the simulation box. This quantity equals 1 when the vector E_i^{u2} is extended over the whole system, and decreases progressively as the spatial localization of E_i^{u2} becomes more pronounced. The participation ratio is defined as

$$p^u = \left(N \sum_{i=1}^{N} E_i^{u4} \right)^{-1}, \tag{14}$$

and provides a rough estimate of the fraction of particles having significant displacements in E_i^{u2}. For instance, p^u should be $O(1)$ when the unstable modes are homogeneously distributed in the system. The temperature dependence of these two quantities is shown in Fig. 11 for different Lennard-Jones mixtures. The existence of a sharp localization of unstable modes around T_r, as identified by the abrupt decrease of $L^u(T)$, appears to be a universal feature of

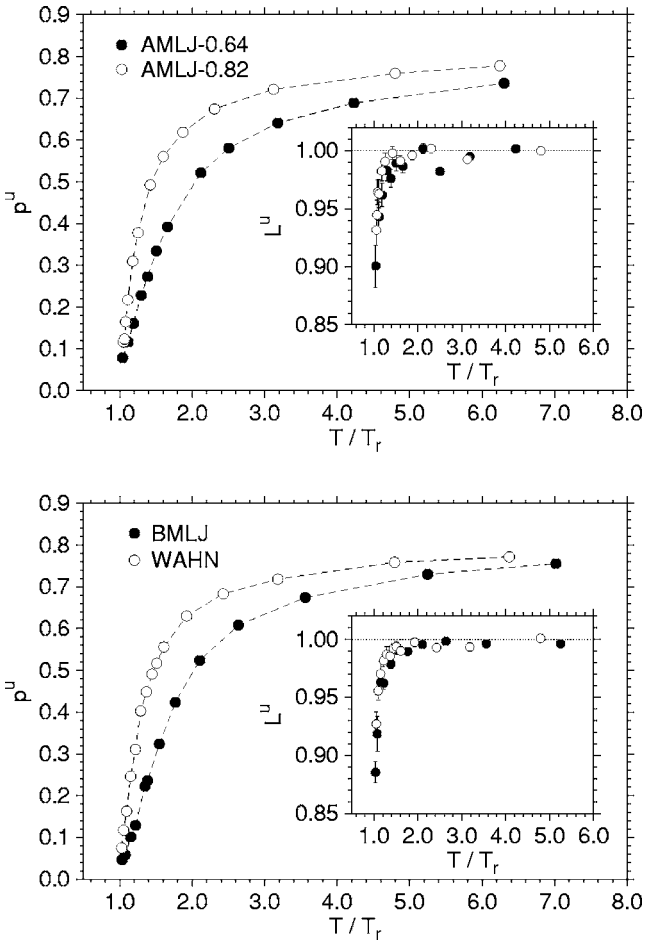

FIG. 11. Participation ratio p^u of average squared displacements on unstable modes as a function of reduced temperature T/T_r at $P=10$. Insets show the reduced gyration radius L_u against T/T_r. Upper plot: AMLJ-0.82 (white squares) and AMLJ-0.64 (black squares). Lower plot: WAHN (white circles) and BMLJ (black circles).

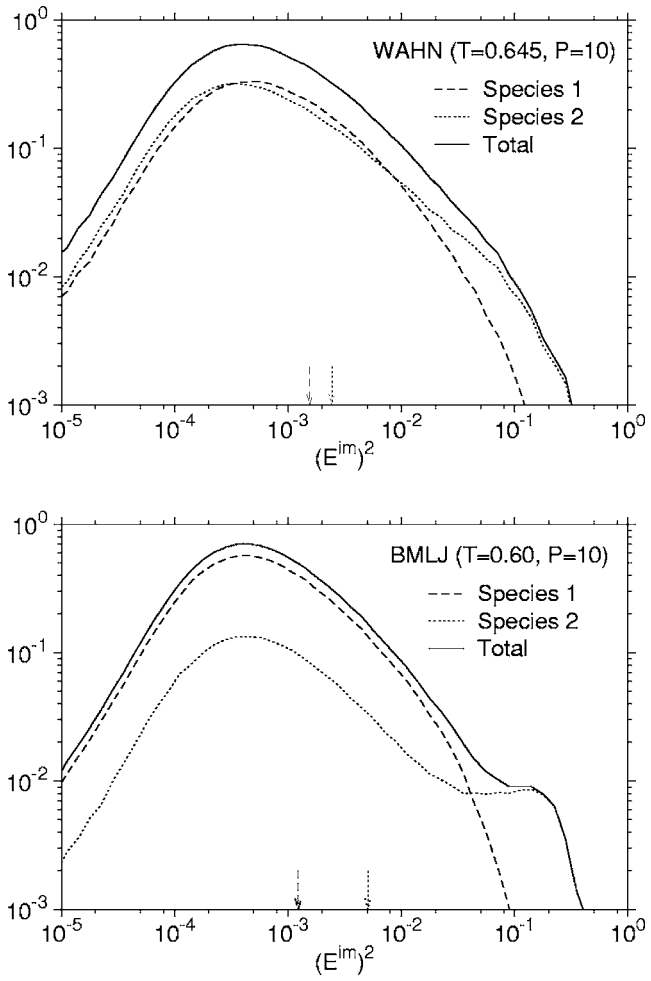

FIG. 12. Distribution of average squared displacements on unstable modes of saddles. Results are shown for small particles (dotted lines), large particles (dashed lines), and irrespective of chemical species (solid lines). Normalization is such that the area under each curve is proportional to the corresponding number concentration. Arrows indicate the average values of $(E_i^u)^2$ for large and small particles. Upper plot: WAHN at $T=0.645$, $P=10$. Lower plot: BMLJ at $T=0.60$, $P=10$.

saddles sampled by supercooled Lennard-Jones mixtures. On the other hand, the pattern of localization of the unstable modes changes according to the fragility of the mixture. The more fragile the mixture, the more rapid the localization of unstable modes upon supercooling, as is suggested by the behavior of $p^u(T)$. In the range of temperature above T_r, we find that fragile mixtures tend to have larger values of p^u. In this case, a larger fraction of particles is thus involved in the unstable modes, which is consistent with the expectation that rearrangements should involve larger clusters as fragility increases.[59] We found further support to these considerations by analyzing the average participation ratio and gyration radius of individual unstable modes of saddles.

Inspection of animated unstable modes of saddles sampled at low temperature indicates the occurrence in BMLJ of strongly localized, high-frequency unstable modes, in which few small particles show very large displacements. This feature is reflected in a clearly bimodal distribution of E_i^{u2} for small particles in deeply supercooled BMLJ. In Fig. 12, we show the distributions of E_i^{u2} for BMLJ and WAHN at the lowest equilibrated temperatures. In the case of BMLJ, in fact, we find a bump at large values in the distribution of E_i^{u2} for small particles. We also often observed correlated, string-like rearrangements of large particles in the unstable modes of BMLJ. This feature is exemplified in the snapshots of Fig. 13, where we show the unstable modes of a typical quasi-saddle sampled in deeply supercooled BMLJ. By comparison, unstable modes in WAHN tend to involve larger and more compact clusters of particles and to possess a more pronounced spatial overlap. These features, in the light of our previous investigations,[23] should influence the dynamical processes within the β-relaxation time scale, and could provide the basis for understanding the microscopic origin of dynamical heterogeneities[60] on longer time scales. Analysis of the connectivity between stationary points could also help explaining the relative weight of different dynamical processes (stringlike motions,[61,62] democratic rearrangements[63]) observed in supercooled Lennard-Jones mixtures. More detailed studies along this direction will require significant additional work.

V. CONCLUSIONS

Molecular dynamics simulations of supercooled Lennard-Jones mixtures continue to provide a useful bench-

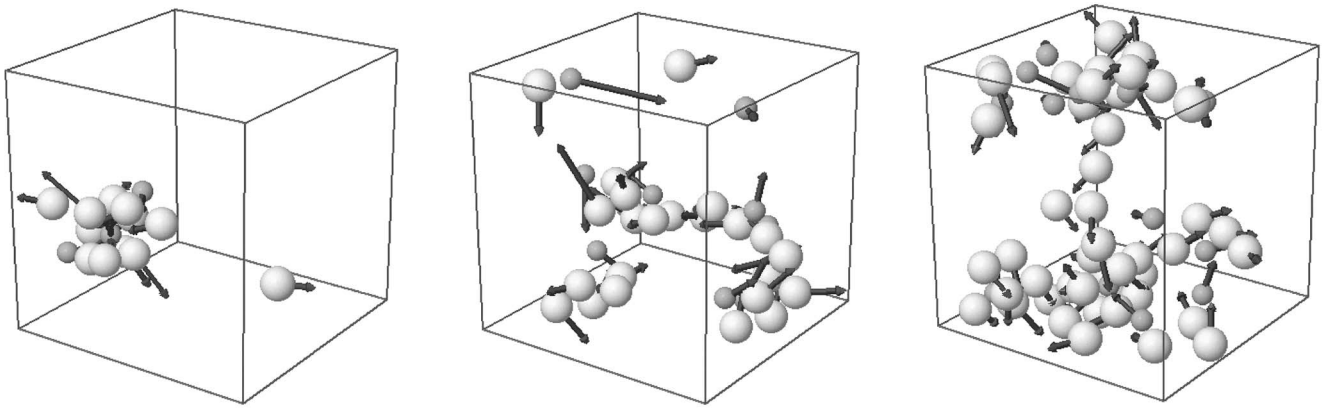

FIG. 13. Selection of three unstable modes of a quasisaddle (n_v=4) sampled in BMLJ at T=0.66, P=10. The nearly zero mode of the quasisaddle has been ignored. A fourth unstable mode, not shown, is very similar in extension and shape to that shown in (b). For clarity, only particles having square displacements $(\boldsymbol{e}_i^u)^2$ larger than 0.004 are shown, and eigenvectors are scaled logarithmically. Large and small particles are shown as pale large spheres and small darker spheres, respectively. Note the strong localization of mode (a) and the existence of distinct stringlike instabilities of large particles in modes (b) and (c).

mark for theories and paradigms of the glass-transition. A minimal exploration of the field of parameters of the Lennard-Jones potential for binary mixtures has revealed a rich phenomenology. In particular, we found a systematic variation of fragility, i.e., a varying degree of super-Arrhenius behavior of dynamical properties. By analyzing the temperature dependence of effective activation energies for relaxation, we found that fragility increases by increasing size ratio $\lambda=\sigma_{22}/\sigma_{11}$ in equimolar, additive mixtures. Two prototypical mixtures, the BMLJ mixture of Kob and Andersen[35] and the one of Wahnström,[39] also have different fragility indexes. As an interesting result, we also found that fragility does not change appreciably with pressure in BMLJ.

In a previous paper,[34] we discussed these trends in terms of the thermal rate of growth of locally preferred structures upon supercooling. Here, we have investigated the different, complementary role of the potential energy surface explored in the supercooled regime. We have adopted a simple, nontopographic approach and analyzed some statistical properties of the PES, with particular focus on high-order stationary points. We have provided an estimate of average potential energy barriers and found a striking correlation with the fragility of the mixture: the more fragile the mixture, the more pronounced the increase of energy barriers upon supercooling. Not ignoring the role of metabasins[6] and multistep processes,[15] an increase of energy barriers between single saddles appears to be a simple, possible mechanism for super-Arrhenius behavior of dynamical properties in fragile glass-formers. We have also found that a proper characterization of the saddles' density of states will already encode the relevant information about fragility. On the other hand, mean frequencies of stable and unstable modes do not provide robust correlations to fragility. Their strong variations with density along different isobars in BMLJ, in fact, are not accompanied by a significant change in fragility.

As a general rule, unstable modes of saddles become more and more localized upon supercooling, but this feature is sharper and more pronounced the more fragile the mixture. This can be interpreted as the counterpart of a more rapid growth, upon supercooling, of slow domains, characterized by distinct locally preferred structures.[34] From some preliminary calculations, we have found, as expected, that particles at the center of locally preferred structures are stabilized and are not involved in the unstable modes. Thus, the study of the potential energy surface presented in this work and our previous microstructural analysis[34] complement each other very well. Formation of stable, long-lived structures, such as icosahedral domains in additive mixtures, could correspond to deeper traps in the energy landscape, thus forcing relaxation over larger energy barriers. On the other hand, frustration of stable prismatic domains could be the origin of the limited growth of potential energy barriers in BMLJ. The two approaches together may thus provide an intriguing picture of the fragile versus strong behavior of glass-former, bridging the ideas of frustration in supercooled liquids[64] and roughness of the energy landscape.[10] Assessment of such picture by studying different interactions remains an open problem for further investigations.

ACKNOWLEDGMENTS

The authors would like to thank A. Cavagna for useful discussions and a critical reading of the manuscript. Computational resources for the present work have been partly obtained through a grant from "Iniziativa Trasversale di Calcolo Parallelo" of the Italian *CNR-Istituto Nazionale per la Fisica della Materia* (CNR-INFM) and partly within the agreement between the University of Trieste and the Consorzio Interuniversitario CINECA (Italy).

[1] F. Sciortino, J. Stat. Mech.: Theory Exp. **2005**, P05015 (2005).
[2] D. J. Wales, *Energy Landscapes* (Cambridge University Press, Cambridge, 2003).
[3] F. H. Stillinger and T. A. Weber, Phys. Rev. A **25**, 978 (1982).
[4] S. Sastry, P. G. Debenedetti, and F. H. Stillinger, Nature **393**, 554 (1998).
[5] F. H. Stillinger, Phys. Rev. B **41**, 2409 (1990).
[6] B. Doliwa and A. Heuer, Phys. Rev. Lett. **91**, 235501 (2003).
[7] B. Doliwa and A. Heuer, Phys. Rev. E **67**, 031506 (2003).
[8] B. Doliwa and A. Heuer, Phys. Rev. E **67**, 030501 (2003).
[9] R. A. Denny, D. R. Reichman, and J.-P. Bouchaud, Phys. Rev. Lett. **90**,

025503 (2003).
[10] F. H. Stillinger, Science **267**, 1935 (1995).
[11] S. Sastry, Nature **409**, 164 (2001).
[12] R. J. Speedy, J. Phys. Chem. B **103**, 4060 (1999).
[13] G. Ruocco, F. Sciortino, F. Zamponi, C. De Michele, and T. Scopigno, J. Chem. Phys. **120**, 10666 (2004).
[14] G. Tarjus, D. Kivelson, S. Mossa, and C. Alba-Simionesco, J. Chem. Phys. **120**, 6135 (2004).
[15] T. F. Middleton and D. J. Wales, Phys. Rev. B **64**, 024205 (2001).
[16] T. F. Middleton and D. J. Wales, J. Chem. Phys. **118**, 4583 (2003).
[17] L. Angelani, G. Ruocco, M. Sampoli, and F. Sciortino, J. Chem. Phys. **119**, 2120 (2003).
[18] J. P. K. Doye and D. J. Wales, J. Chem. Phys. **116**, 3777 (2002).
[19] D. J. Wales and J. P. K. Doye, J. Chem. Phys. **119**, 12409 (2003).
[20] M. Sampoli, P. Benassi, R. Eramo, L. Angelani, and G. Ruocco, J. Phys.: Condens. Matter **15**, S1227 (2003).
[21] L. Angelani, R. Di Leonardo, G. Ruocco, A. Scala, and F. Sciortino, Phys. Rev. Lett. **85**, 5356 (2000).
[22] L. Angelani, R. Di Leonardo, G. Ruocco, A. Scala, and F. Sciortino, J. Chem. Phys. **116**, 10297 (2002).
[23] D. Coslovich and G. Pastore, Europhys. Lett. **75**, 784 (2006).
[24] A. Cavagna, Europhys. Lett. **53**, 490 (2001).
[25] F. Zamponi, L. Angelani, L. F. Cugliandolo, J. Kurchan, and G. Ruocco, J. Phys A **36**, 8565 (2004).
[26] T. Keyes, J. Chowdhary, and J. Kim, Phys. Rev. E **66**, 051110 (2002).
[27] A. Andronico, L. Angelani, L. F. Cugliandolo, J. Kurchan, and G. Ruocco, Phys. Rev. E **70**, 041101 (2004).
[28] A. Cavagna, I. Giardina, and G. Parisi, J. Phys A **34**, 5317 (2001).
[29] T. Grigera, A. Cavagna, I. Giardina, and G. Parisi, Phys. Rev. Lett. **88**, 055502 (2002).
[30] P. Shah and C. Chakravarty, J. Chem. Phys. **115**, 8784 (2001).
[31] S. N. Chakraborty and C. Chakravarty, J. Chem. Phys. **124**, 014507 (2006).
[32] L. Angelani, C. De Michele, G. Ruocco, and F. Sciortino, J. Chem. Phys. **121**, 7533 (2004).
[33] C. De Michele, F. Sciortino, and A. Coniglio, J. Phys.: Condens. Matter **16**, L489 (2004).
[34] D. Coslovich and G. Pastore, J. Chem. Phys. **127**, 124504 (2007).
[35] W. Kob and H. C. Andersen, Phys. Rev. E **51**, 4626 (1995).
[36] W. Kob and H. C. Andersen, Phys. Rev. E **52**, 4134 (1995).
[37] S. D. Stoddard and J. Ford, Phys. Rev. A **8**, 1504 (1973).
[38] P. Shah and C. Chakravarty, J. Chem. Phys. **118**, 2342 (2003).
[39] G. Wahnström, Phys. Rev. A **44**, 3752 (1991).
[40] S. D. Bond, B. J. Leimkuhler, and B. B. Laird, J. Comput. Phys. **151**, 114 (1999).
[41] S. Nosé, J. Phys. Soc. Jpn. **70**, 75 (2001).
[42] M. P. Allen and D. J. Tildesley, *Computer Simulation of Liquids* (Clarendon, London, 1987).
[43] D. C. Liu and J. Nocedal, Math. Program. **45**, 503 (1989).
[44] T. S. Grigera, J. Chem. Phys. **124**, 064502 (2006).
[45] D. Kivelson, G. Tarjus, X. Zhao, and S. A. Kivelson, Phys. Rev. E **53**, 751 (1996).
[46] M. L. Ferrer, H. Sakai, D. Kivelson, and C. Alba-Simionesco, J. Phys. Chem. B **103**, 4191 (1999).
[47] G. Tarjus, D. Kivelson, and P. Viot, J. Phys.: Condens. Matter **12**, 6497 (2000).
[48] V. N. Novikov, Y. Ding, and A. P. Sokolov, Phys. Rev. E **71**, 061501 (2005).
[49] C. A. Angell, B. E. Richards, and V. Velikov, J. Phys.: Condens. Matter **11**, A75 (1999).
[50] S. D. Bembenek and B. B. Laird, J. Chem. Phys. **104**, 5199 (1995).
[51] J. D. Gezelter, E. Rabani, and B. J. Berne, J. Chem. Phys. **107**, 4618 (1997).
[52] T. Keyes, G. V. Vijayadamodar, and U. Zurcher, J. Chem. Phys. **106**, 4651 (1997).
[53] K. Broderix, K. K. Bhattacharya, A. Cavagna, A. Zippelius, and I. Giardina, Phys. Rev. Lett. **85**, 5360 (2000).
[54] A. Cavagna, I. Giardina, and T. Grigera, J. Phys A **36**, 10721 (2003).
[55] T. Keyes, J. Chem. Phys. **101**, 5081 (1995).
[56] G. Vijayadamodar and A. Nitzan, J. Chem. Phys. **103**, 2169 (1995).
[57] W.-X. Li and T. Keyes, J. Chem. Phys. **111**, 5503 (1999).
[58] L. Berthier and J. P. Garrahan, Phys. Rev. E **68**, 041201 (2003).
[59] E. A. Jagla, Mol. Phys. **99**, 753 (2001).
[60] A. Widmer-Cooper, P. Harrowell, and H. Fynewever, Phys. Rev. Lett. **93**, 135701 (2004).
[61] C. Donati, S. C. Glotzer, P. H. Poole, S. J. Plimpton, and W. Kob, Phys. Rev. E **60**, 3107 (1999).
[62] T. B. Schrøder, S. Sastry, J. C. Dyre, and S. C. Glotzer, J. Chem. Phys. **112**, 9834 (2000).
[63] G. A. Appignanesi, J. A. Rodriguez Fris, R. A. Montani, and W. Kob, Phys. Rev. Lett. **96**, 057801 (2005).
[64] G. Tarjus, S. A. Kivelson, Z. Nussinov, and P. Viot, J. Phys.: Condens. Matter **17**, R1143 (2005).
[65] J. Chowdhary and T. Keyes, Physica A **314**, 575 (2002).
[66] Actually, also a third way has been considered (Ref. 65).
[67] Introduction of a lower frequency cutoff ω_c to filter some shoulder modes (Ref. 57) would not affect our conclusions.
[68] It has been suggested (Ref. 16) that the leading contribution to the density dependence of the geometric mean frequency in local minima should scale as a power law of ρ. We argue that a similar argument might hold for high-order stationary points.